# Thermodynamic uncertainty relations and molecular-scale energy conversion

M. W. Jack [*] and N. J. López-Alamilla
*Department of Physics, University of Otago, Dunedin, New Zealand*

K. J. Challis
*Scion, 49 Sala Street, Rotorua 3046, New Zealand*

The thermodynamic uncertainty relation (TUR) is a universal constraint for nonequilibrium steady states that requires the entropy production rate to be greater than the relative magnitude of current fluctuations. It has potentially important implications for the thermodynamic efficiency of molecular-scale energy conversion in both biological and artificial systems. An alternative multidimensional thermodynamic uncertainty relation (MTUR) has also been proposed. In this paper we apply the TUR and the MTUR to a description of molecular-scale energy conversion that explicitly contains the degrees of freedom exchanging energy via a time-independent multidimensional periodic potential. The TUR and the MTUR are found to be universal lower bounds on the entropy generation rate and provide upper bounds on the thermodynamic efficiency. The TUR is found to provide only a weak bound while the MTUR provides a much tighter constraint by taking into account correlations between degrees of freedom. The MTUR is found to provide a tight bound in the near or far from equilibrium regimes but not in the intermediate force regime. Collectively, these results demonstrate that the MTUR is more appropriate than the TUR for energy conversion processes, but that both diverge from the actual entropy generation in certain regimes.

## I. INTRODUCTION

The thermodynamic uncertainty relation (TUR) is a fundamental relationship between the relative uncertainty in position and entropy production in nonequilibrium steady states [1,2]. The TUR can be interpreted to mean that "small relative fluctuations come at the cost of more dissipation." The TUR has been applied to a diverse range of nonequilibrium systems illustrating the trade-off between dissipation and precision [3–7]. The ramifications of the TUR for the efficiency of molecular-scale energy conversion [8–10] has also been considered. In addition, very recently an alternative multidimensional uncertainty relation (MTUR) has also been derived [11]. In this paper we consider a model of energy conversion that explicitly describes the two degrees of freedom exchanging energy and evaluate the TUR and the MTUR bounds on the entropy production and efficiency in a wide range of nonequilibrium regimes.

Molecular-scale energy conversion can be formulated in terms of the multidimensional Smoluchowski equation describing overdamped Brownian motion on a potential surface [12,13]:

$$\frac{\partial P(\boldsymbol{r}, t)}{\partial t} = \mathcal{L} P(\boldsymbol{r}, t), \qquad (1)$$

$$\mathcal{L} = \nabla^{\mathsf{T}} M [\nabla V(\boldsymbol{r}) + k_B T \nabla], \qquad (2)$$

where $\mathcal{L}$ is the evolution operator, $k_B$ is Boltzman's constant, $T$ is the temperature, and $M$ is a diagonal matrix of inverse

---

*Corresponding author: michael.jack@otago.ac.nz

friction coefficients $M_{jj} = \gamma_j^{-1}$. The probability to find the system in the state given by the continuous variable $\boldsymbol{r}$ is denoted $P(\boldsymbol{r}, t)$. We assume a time-independent potential of the form

$$V(\boldsymbol{r}) = V_0(\boldsymbol{r}) - \boldsymbol{f}^{\mathsf{T}} \boldsymbol{r}, \qquad (3)$$

where $V_0(\boldsymbol{r}) = V_0(\boldsymbol{r} + \boldsymbol{a})$ is periodic, with periodicity $\boldsymbol{a}$ and $\boldsymbol{f}$ is a constant macroscopic force driving the system out of thermal equilibrium. When the periodic potential is nonseparable, energy can be converted between degrees of freedom [12]. For example, mechanochemical energy conversion and transduction processes can be described by Eq. (1) in two dimensions, where $\boldsymbol{r} = (x, y)$ with $y$ representing a chemical degree of freedom (i.e., a reaction coordinate) and $x$ a mechanical degree of freedom.

In the limit of deep potential wells, Eq. (1) can be approximated by a simpler discrete master equation describing thermally activated hopping between potential wells [14]:

$$\frac{dp_n(t)}{dt} = \sum_m \left[ \kappa_{n,m} p_m(t) - \kappa_{m,n} p_n(t) \right], \qquad (4)$$

where $\kappa_{n,m}$ are hopping rates from well $m$ to $n$, determined by the underlying potential. A number of authors use Eq. (4) as a starting point for treating molecular-scale energy conversion and impose constraints on $\kappa_{n,m}$ to ensure thermodynamic consistency [15]. In this paper we use Eq. (4) within its regime of validity, and use the more general formulation in Eq. (1) to explore a range of potentials where the discrete master equation is not valid.

For $\boldsymbol{f} \neq 0$, Eq. (1) has a nonequilibrium steady state. Two quantities that characterize this state are the drift and the diffusion matrix:

$$\boldsymbol{v} \equiv \lim_{t \to \infty} \frac{\langle \boldsymbol{r}(t) \rangle}{t}, \tag{5}$$

$$D \equiv \lim_{t \to \infty} \frac{\langle [\boldsymbol{r}(t) - \langle \boldsymbol{r}(t) \rangle][\boldsymbol{r}(t) - \langle \boldsymbol{r}(t) \rangle]^{\mathsf{T}} \rangle}{2t}. \tag{6}$$

The diffusion matrix $D$ is symmetric and positive semidefinite [16]. It provides a measure of both the fluctuations and the correlations of the degrees of freedom. A consistent thermodynamics can be developed for the nonequilibrium system described by Eq. (1) [17–19]. In particular, the steady-state second law of thermodynamics becomes

$$\sigma = \frac{\boldsymbol{f}^{\mathsf{T}} \boldsymbol{v}}{T} \geqslant 0, \tag{7}$$

where $\sigma$ is the rate of entropy generation.

The thermodynamic uncertainty relation (TUR) was first conjectured in Ref. [1] and proven for the discrete case described by Eq. (4) in Ref. [2]. It states that the entropy generation is bound from below by

$$\sigma \geqslant \sigma_j^{\mathrm{TUR}} \equiv k_B v_j^2 / D_{jj}, \tag{8}$$

for all $j$. Equation (8) has also been shown to hold for the system described by Eq. (1) in one dimension [20]. The bound (8) has important consequences for energy conversion. To see this note that in two dimensions if $y$ is the driving degree of freedom then the thermodynamic efficiency of energy conversion can be written as [19]

$$\eta = 1 - \frac{T \sigma}{v_y f_y} \leqslant 1. \tag{9}$$

Equation (9) demonstrates that a lower bound on the entropy generation rate equates to an upper bound on the efficiency. The effect of the TUR bound on efficiency has been explored previously [9,10], but this work has not explicitly considered the two degrees of freedom exchanging energy making the results difficult to interpret.

A multidimensional thermodynamic uncertainty relation (MTUR) has been derived using the Crámer-Rao bound from information theory for systems described by Eq. (1) [11]. The MTUR takes the form

$$\sigma \geqslant \sigma^{\mathrm{MTUR}} \equiv k_B \boldsymbol{v}^{\mathsf{T}} D^{-1} \boldsymbol{v}, \tag{10}$$

and incorporates the full diffusion matrix. In this paper we aim to compare the MTUR to the TUR focusing in particular on the case of molecular-scale energy conversion. This is interesting because energy conversion is intrinsically multidimensional and gives rise to correlations between degrees of freedom due to the nonseparable potential [21]. In addition, as Eq. (1) has a wider regime of validity than Eq. (4), it can be used to explore entropy generation for a wider range of parameters. In particular, it describes the critical point where $|\boldsymbol{f}^{\mathsf{T}} \boldsymbol{a}|$ is large enough that potential barriers between adjacent wells vanish and the far from equilibrium case where $|\boldsymbol{f}^{\mathsf{T}} \boldsymbol{a}|$ is much larger than the barriers in $V_0(\boldsymbol{r})$. In both these regimes the description in terms of the master equation becomes invalid [20]. In one dimension it has been shown that the

TUR bound diverges from the entropy generation rate close to the critical point [20]. The current paper aims to explore the MTUR and TUR bounds in two dimensions across all force regimes.

This paper is ordered as follows. Starting from Eq. (1), we briefly summarize a multidimensional formulation of energy conversion (Sec. II). We then provide an interpretation of the MTUR as a coarse-grained entropy production rate (Sec. III). Next we show that the MTUR is always a tighter bound on the entropy generation than the TUR (Sec. IV). We then evaluate the deep well case when the system Eq. (1) can be described by Eq. (4) and an analytical solution for the drift and diffusion matrix exists (Sec. V). Finally, we show numerical results for potentials beyond the deep well regime where analytical solutions do not exist (Sec. VI). These last two sections will compare the actual entropy generation, $\sigma$, with the MTUR ($\sigma^{\mathrm{MTUR}}$) and TUR ($\sigma_j^{\mathrm{TUR}}$) bounds and the implied bounds on efficiency.

## II. BACKGROUND

We take as our starting point the multidimensional Smoluchowski equation (1) describing overdamped Brownian motion on a potential surface. We define a probability current as $\boldsymbol{J}(\boldsymbol{r}, t) = -M[\boldsymbol{\nabla} V(\boldsymbol{r}) + k_B T \boldsymbol{\nabla}] P(\boldsymbol{r}, t)$. In the steady state when $\boldsymbol{f} = 0$, $\boldsymbol{J}^{\mathrm{ss}}(\boldsymbol{r}) = 0$ everywhere and $P_{\mathrm{ss}}(\boldsymbol{r}) \propto e^{-V(\boldsymbol{r})/k_B T}$ takes the usual Boltzmann form. When $\boldsymbol{f} \neq 0$, the system is in a nonequilibrium steady state and we have $\boldsymbol{\nabla}^{\mathsf{T}} \boldsymbol{J}_{\mathrm{ss}}(\boldsymbol{r}) = 0$ which, for general potentials, only yields analytical solutions in one dimension [20,22].

Defining the internal energy and the Shannon entropy by

$$U(t) \equiv \int d\boldsymbol{r} \, P(\boldsymbol{r}, t) V(\boldsymbol{r}), \tag{11}$$

$$S(t) \equiv -k_B \int d\boldsymbol{r} \, P(\boldsymbol{r}, t) \ln P(\boldsymbol{r}, t), \tag{12}$$

respectively, we can derive a consistent thermodynamics for the system [17–19]. In the steady state, the first law of thermodynamics becomes

$$\boldsymbol{f}^{\mathsf{T}} \boldsymbol{v} = - \int_{\mathcal{A}} d\boldsymbol{r} \, [\boldsymbol{J}^{\mathrm{ss}}(\boldsymbol{r})]^{\mathsf{T}} \boldsymbol{\nabla} V(\boldsymbol{r}), \tag{13}$$

where the integral is over one period, represented by $\mathcal{A}$. The terms on the left-hand side of Eq. (13) can be recognized as the rate of work input to the system and the terms of the right-hand side the rate of heat output from the system. The second law of thermodynamics in the steady state is given by Eq. (7) where the entropy generation rate is defined by

$$\sigma \equiv \int_{\mathcal{A}} d\boldsymbol{r} \, \frac{[\boldsymbol{J}^{\mathrm{ss}}(\boldsymbol{r})]^{\mathsf{T}} M^{-1} \boldsymbol{J}^{\mathrm{ss}}(\boldsymbol{r})}{T P_{\mathrm{ss}}(\boldsymbol{r})} \geqslant 0. \tag{14}$$

Recognizing $f_j v_j$ as the rates of work into the system, if $f_y v_y > 0$ and $y$ is the driving degree of freedom (e.g., the chemical degree of freedom), then energy conversion requires $f_x v_x < 0$, where $x$ is the driven degree of freedom (e.g., the mechanical degree of freedom) in two dimensions. The thermodynamic efficiency of energy conversion between two

degrees of freedom when $f_x, f_y \neq 0$ is given by

$$\eta \equiv -\frac{v_x f_x}{v_y f_y}. \tag{15}$$

Equation (9) is derived from Eq. (15) using Eq. (7). In contrast, the Stokes efficiency [23]

$$\varepsilon \equiv \frac{\gamma_x v_x^2}{f_y v_y} \tag{16}$$

represents a measure of the motion induced in the $x$ coordinate when $f_x = 0$ by a force in $y$. The Stoke's efficiency $\varepsilon$ can also be written in terms of the entropy generation rate (with $f_x = 0$) as

$$\varepsilon \equiv \frac{\gamma_x v_x^2}{T \sigma}, \tag{17}$$

such that a lower bound on $\sigma$ will again lead to an upper bound on $\varepsilon$.

Similar to an electron in a periodic potential [24], the periodicity of $\nabla V(\boldsymbol{r})$, means that a formal solution to Eq. (1) can be written as

$$P(\boldsymbol{r}, t) = \sum_\alpha \int_{\mathcal{B}} d\boldsymbol{k} \, c_{\boldsymbol{k},\alpha} \phi_{\boldsymbol{k},\alpha}(\boldsymbol{r}) e^{-\lambda_{\boldsymbol{k},\alpha} t}, \tag{18}$$

where the integral is over the first Brillouin zone $\mathcal{B}$, $\boldsymbol{k}$ is the wave number defined on $-\pi/a_j \leqslant k_j \leqslant \pi/a_j$, and $\alpha$ is the band index. The eigenfunctions $\phi_{\boldsymbol{k},\alpha}(\boldsymbol{r})$ satisfy

$$\mathcal{L}\phi_{\boldsymbol{k},\alpha}(\boldsymbol{r}) = -\lambda_{\boldsymbol{k},\alpha}\phi_{\boldsymbol{k},\alpha}(\boldsymbol{r}) \tag{19}$$

and have the Bloch form

$$\phi_{\boldsymbol{k},\alpha}(\boldsymbol{r}) = e^{i\boldsymbol{k}^\top \boldsymbol{r}} u_{\boldsymbol{k},\alpha}(\boldsymbol{r}), \tag{20}$$

where $u_{\boldsymbol{k},\alpha}(\boldsymbol{r}) = u_{\boldsymbol{k},\alpha}(\boldsymbol{r} + \boldsymbol{a})$. The (complex-valued) eigenvalues $\lambda_{\boldsymbol{k},\alpha}$ have the structure $\mathrm{Re}\{\lambda_{\boldsymbol{k},0}\} < \mathrm{Re}\{\lambda_{\boldsymbol{k},1}\} < \mathrm{Re}\{\lambda_{\boldsymbol{k},2}\} < \cdots$. This Bloch state description will be used in Sec. III to provide a physical interpretation of the MTUR.

In the case of deep wells, the Bloch state description in Eq. (18) can be used to transform the continuous description given by Eq. (1) to a simplified discrete description [14]. In the limit of deep wells, there is a large band gap between $\alpha = 0$ and $\alpha > 0$ states representing a time-scale separation in the dynamics. This enables the bands with $\alpha > 0$ to be adiabatically eliminated and we can write $P(\boldsymbol{r}, t) \approx \sum p_n(t)\omega_n(\boldsymbol{r})$, where $\omega_n(\boldsymbol{r})$ is a state localized at the $n$th well and $p_n(t)$ is the probability of occupying that state. The evolution can then be approximated by Eq. (4). Generalizations of this derivation have also been carried out for discrete-continuous systems [25].

In the special case of a single well per period, the eigenvalues and the hopping rates are related by [14]

$$\lambda_{\boldsymbol{k},0} = -\sum_{\langle \boldsymbol{m},\boldsymbol{n} \rangle} \kappa_{\boldsymbol{n},\boldsymbol{m}} e^{-i\boldsymbol{k}^\top A(\boldsymbol{n}-\boldsymbol{m})}, \tag{21}$$

$$\kappa_{\boldsymbol{n},\boldsymbol{m}} = -\frac{a_x a_y}{(2\pi)^2} \int_B d\boldsymbol{k} \, \lambda_{\boldsymbol{k},0} e^{i\boldsymbol{k}^\top A(\boldsymbol{n}-\boldsymbol{m})}, \tag{22}$$

where $A$ is a diagonal matrix with $A_{jj} = a_j$ and the summation in Eq. (21) is over nearest neighbors. It is possible to show that the above derivation ensures that $\kappa_{\boldsymbol{n},\boldsymbol{m}}/\kappa_{\boldsymbol{m},\boldsymbol{n}} = e^{f^\top A(\boldsymbol{n}-\boldsymbol{m})/k_B T}$, which is required for thermodynamic consistency. In the deep

well regime the hopping rates are well approximated by Kramer's rate where the relative height of the nearest saddle points affect the rates via

$$\kappa_{\boldsymbol{n},\boldsymbol{m}} \approx e^{-[V^0(\boldsymbol{r}_n) - V^0(\boldsymbol{s}_{n,m}) - f^\top A\alpha_{n-m}(\boldsymbol{n}-\boldsymbol{m})]/k_B T}, \tag{23}$$

where $\boldsymbol{r}_n$ is the position of the minimum of the $n$th well, $\boldsymbol{s}_{n,m}$ is the position of the saddle point between the $\boldsymbol{n}$ and $\boldsymbol{m}$th wells, and $A\alpha_{n-m}(\boldsymbol{n}-\boldsymbol{m}) = \boldsymbol{r}_n - \boldsymbol{s}_{n,m}$ such that $0 \leqslant \alpha_{n-m} \leqslant 1$ and $\alpha_{n-m} + \alpha_{m-n} = 1$. In general, $\alpha_{m-n}$ is a function of external force. Further approximating $\kappa_{\boldsymbol{n},\boldsymbol{m}} \approx \kappa^0_{n-m} e^{\alpha^0_{n-m} f^\top A(\boldsymbol{n}-\boldsymbol{m})/k_B T}$, where $\kappa^0_{n-m}$ and $\alpha^0_{n-m}$ are the values at equilibrium ($\boldsymbol{f} = 0$), we can write an explicit expression for the $\lambda_{\boldsymbol{k},0}$ as a function of the applied force $\boldsymbol{f}$. This is given by Eq. (A1) in Appendix A and will be used in Sec. V to compare the TUR and the MTUR.

## III. COARSE-GRAINED DESCRIPTION

We present an interpretation of the MTUR given by Eq. (10). In the long-time limit, the system is dictated by states close to $\boldsymbol{k} = 0$, $\alpha = 0$, and, for a length scale much larger than the periodicity of the lattice, we can neglect the $\alpha > 0$ bands and make the replacement $u_{\boldsymbol{k},0}(\boldsymbol{r}) \approx 1$ in Eq. (18) to define a coarse-grained probability by

$$\tilde{P}(\boldsymbol{r}, t) \approx \int d\boldsymbol{k} \, c_{\boldsymbol{k},0} e^{i\boldsymbol{k}^\top \boldsymbol{r} - \lambda_{\boldsymbol{k},0} t}, \tag{24}$$

where the integral is now over all $\boldsymbol{k}$ space. Recognizing $c_{\boldsymbol{k},0} e^{-\lambda_{\boldsymbol{k},0} t}$ as a characteristic function [16,21] for $\tilde{P}(\boldsymbol{r}, t)$ we can show that

$$\boldsymbol{v} = i\nabla_{\boldsymbol{k}}\lambda_{\boldsymbol{k},0}\big|_{\boldsymbol{k}=0}, \tag{25}$$

$$D = \tfrac{1}{2}\nabla_{\boldsymbol{k}}\nabla_{\boldsymbol{k}}\lambda_{\boldsymbol{k},0}\big|_{\boldsymbol{k}=0}. \tag{26}$$

Truncating the eigenvalues at quadratic order in $\boldsymbol{k}$, we can approximate the coarse-grained probability as

$$\tilde{P}(\boldsymbol{r}, t) \approx \int d\boldsymbol{k} \, c_{\boldsymbol{k},0} e^{i\boldsymbol{k}^\top(\boldsymbol{r}-\boldsymbol{v}t) - \boldsymbol{k}^\top D\boldsymbol{k}t}, \tag{27}$$

which is equivalent to a coarse-grained evolution in terms of a global drift and diffusion:

$$\frac{\partial \tilde{P}(\boldsymbol{r}, t)}{\partial t} = \nabla^\top[-\boldsymbol{v} + D\nabla]\tilde{P}(\boldsymbol{r}, t). \tag{28}$$

Defining the Shannon entropy for $\tilde{P}(\boldsymbol{r}, t)$ similar to Eq. (12), we can also develop a consistent thermodynamics for this coarse-grained system following the same procedure as in Ref. [17]. For the physically relevant case where $D$ is positive definite (which implies that $D^{-1}$ is also positive definite), the coarse-grained entropy generation rate is

$$\tilde{\sigma} \equiv k_b \int d\boldsymbol{r} \frac{[\tilde{\boldsymbol{J}}_{ss}(\boldsymbol{r})]^\top D^{-1}\tilde{\boldsymbol{J}}_{ss}(\boldsymbol{r})}{\tilde{P}_{ss}(\boldsymbol{r})} \geqslant 0, \tag{29}$$

where $\tilde{\boldsymbol{J}}_{ss}(\boldsymbol{r}) = [\boldsymbol{v} - D\nabla]\tilde{P}_{ss}(\boldsymbol{r})$ and we have assumed that the probability vanishes at infinity. The steady-state second law of thermodynamics then becomes

$$\tilde{\sigma} = k_B \boldsymbol{v}^\top D^{-1}\boldsymbol{v} = \sigma^{\mathrm{MTUR}}, \tag{30}$$

enabling $\sigma^{\text{MTUR}}$ to be interpreted as the coarse-grained entropy generation rate and the MTUR bound (10) the requirement that the actual entropy generation rate is always greater than the coarse-grained entropy generation rate. Note that, in one dimension, we have $v = J_{ss}a$, $\sigma = (\gamma v^2/a^2 T) \int_0^a dx \, P_{ss}^{-1}(x)$ and the inequality Eq. (10) can be rewritten as

$$\frac{\gamma D}{k_B T a^2} \int_0^a dx \, P_{ss}^{-1}(x) \geqslant 1, \quad (31)$$

which agrees with Ref. [20].

An alternative interpretation of the MTUR bound in terms of the relative uncertainty is also possible. Writing the TUR as $\sigma D_{xx}/v_x^2 \geqslant k_B$, for a position coordinate $x$, the TUR has been interpreted as meaning that greater dissipation is required in order to achieve less relative uncertainty in position: $D_{xx}/v_x^2$. Solving Eq. (28) for an initial state localized in configuration space, we get

$$\tilde{P}(\boldsymbol{r}, t) \propto \exp\left\{-\frac{1}{4t}(\boldsymbol{r} - \boldsymbol{v}t)^{\mathsf{T}} D^{-1}(\boldsymbol{r} - \boldsymbol{v}t)\right\}, \quad (32)$$

which describes a time-varying multivariate Gaussian undergoing drift $\boldsymbol{v}$ and diffusing in multiple dimensions via $D$. Thus $(\boldsymbol{v}^{\mathsf{T}} D^{-1} \boldsymbol{v})^{-1}$ can be interpreted as the relative uncertainty in multidimensional space.

## IV. PROPERTIES OF THE MTUR

Given the forms $\sigma_j^{\text{TUR}} = k_B v_j^2/D_{jj}$ and $\sigma^{\text{MTUR}} = k_B \boldsymbol{v}^{\mathsf{T}} D^{-1} \boldsymbol{v}$ in terms of the drift and the diffusion, it is possible to prove that

$$\sigma^{\text{MTUR}} \geqslant \sigma_j^{\text{TUR}}, \quad (33)$$

for all $j$. The proof is straightforward in two dimensions. Consider the inequality

$$\frac{(v_x D_{xy} - v_y D_{xx})^2}{D_{xx} \det(D)} \geqslant 0, \quad (34)$$

where $D_{xx} \geqslant 0$ and $\det(D) \geqslant 0$ represents the determinant of $D$. Rearranging we can write

$$\frac{v_x^2 D_{yy} + v_y^2 D_{xx} - 2 v_x v_2 D_{xy}}{\det(D)} - \frac{v_x^2}{D_{xx}} \geqslant 0. \quad (35)$$

Recognizing the first fraction as $\boldsymbol{v}^{\mathsf{T}} D^{-1} \boldsymbol{v}$ completes the proof of (33) for the $x$ coordinate. A similar result holds if $x$ is exchanged for $y$ in the above derivation. In Appendix B we provide a proof that (33) also holds in higher dimensions. Thus the MTUR is consistent with the TUR but provides a tighter bound on the entropy generation:

$$\sigma \geqslant \sigma^{\text{MTUR}} \geqslant \sigma_j^{\text{TUR}}. \quad (36)$$

The key difference between the TUR and the MTUR is that the MTUR takes into account correlations between degrees of freedom in the off-diagonal elements of the diffusion matrix. We can explore this difference explicitly in two dimensions by writing

$$k_B \boldsymbol{v}^{\mathsf{T}} D^{-1} \boldsymbol{v} = \frac{k_B D_{xx} D_{yy}}{D_{xx} D_{yy} - D_{xy}^2} \left(\sum_j \frac{v_j^2}{D_{jj}} - 2 \frac{v_x v_y D_{xy}}{D_{xx} D_{yy}}\right). \quad (37)$$

If the off-diagonal elements vanish, then the right-hand side reduces to $\sum_j k_B \frac{v_j^2}{D_{jj}} = \sum_j \sigma_j^{\text{TUR}}$. In contrast, when $D_{xy} \neq 0$, no general rule exists to determine if $k_B \boldsymbol{v}^{\mathsf{T}} D^{-1} \boldsymbol{v}$ is greater or less than $\sum_j \sigma_j^{\text{TUR}}$. The results below show that both cases can occur. Appendix C provides more analysis of the different functional structure of the actual entropy generation, the TUR and the MTUR.

## V. DEEP-WELL REGIME

In the deep-well limit we can derive an analytical expression for the eigenvalue of the lowest band $\lambda_{0,\boldsymbol{k}}$. This is given by Eq. (A1) in Appendix A. From this expression, we can use Eqs. (25) and (26) to derive analytical expressions for the drift (A2) and diffusion (A3). A simplified version of these equations is

$$\frac{v_x}{a_x} = 2\kappa_{(1,0)}^0 \sinh(X_x/2) + 2\kappa_{(1,1)}^0 \sinh(X_+/2), \quad (38a)$$

$$\frac{v_y}{a_y} = 2\kappa_{(0,1)}^0 \sinh(X_y/2) + 2\kappa_{(1,1)}^0 \sinh(X_+/2) \quad (38b)$$

and

$$\frac{D_{xx}}{a_x^2} = \kappa_{(1,0)}^0 \cosh(X_x/2) + \kappa_{(1,1)}^0 \cosh(X_+/2), \quad (39a)$$

$$\frac{D_{yy}}{a_y^2} = \kappa_{(0,1)}^0 \cosh(X_y/2) + \kappa_{(1,1)}^0 \cosh(X_+/2), \quad (39b)$$

$$\frac{D_{xy}}{a_x a_y} = \frac{D_{yx}}{a_x a_y} = \kappa_{(1,1)}^0 \cosh(X_+/2), \quad (39c)$$

where we have defined the dimensionless forces $\boldsymbol{X} = A\boldsymbol{f}/k_B T$ and the quantities $X_{\pm} = X_x \pm X_y$. $\kappa_{(1,0)}^0$ and $\kappa_{(0,1)}^0$ are the rates for "leak" process that do not couple energy, while $\kappa_{(1,1)}^0$ is the rate for coupling transitions. From Eq. (39) it is clear that coupling between the degrees of freedom $\kappa_{(1,1)}^0 \neq 0$ results in $D_{xy} \neq 0$, demonstrating the importance of correlations [21]. High energy conversion can occur in the strong coupling limit: $\kappa_{(1,1)}^0 \gg \kappa_{(1,0)}^0, \kappa_{(0,1)}^0$ when $f_x \approx -f_y$ and $v_x \approx v_y$ [cf. Eq. (15)].

We can use Eqs. (38) and (39) to compare $\sigma$ with the various bounds given in Eqs. (8) and (10). It is useful to consider the relative error, $E = (\sigma - \sigma_B)/\sigma$, and the efficiency bound,

$$\eta_B(\sigma_B) \equiv 1 - \frac{T\sigma_B}{v_y f_y} \geqslant \eta, \quad (40)$$

where $\sigma_B$ is $\sigma^{\text{MTUR}}$ or $\sigma_j^{\text{TUR}}$. The near equilibrium case is shown in Figs. 1 and 2. In Fig. 2 (inset) we can see that $v_x > 0$ for $-0.175 < X_x < 0$, representing an energy conversion process. These plots show that there is close agreement between $\sigma$ and $\sigma^{\text{MTUR}}$ and that the coarse-grained efficiency $\eta_B(\sigma^{\text{MTUR}})$ is indistinguishable from $\eta$. We can understand this from the fact that in this near equilibrium regime $\sinh(X_j/2) \approx X_j/2$ and $\cosh(X_j/2) \approx 1$ and, therefore, $\boldsymbol{v} \approx D(\boldsymbol{f} = 0)\boldsymbol{f}/k_B T$. Rearranging this means that $\boldsymbol{f}^{\mathsf{T}} \boldsymbol{v} \approx k_B T \boldsymbol{v}^{\mathsf{T}} D^{-1} \boldsymbol{v}$ and $\sigma \approx \sigma^{\text{MTUR}}$. In contrast, the $\sigma_j^{\text{TUR}}$ bound does not show close agreement with the full entropy generation or the efficiency. A quadratic increase in the relative error between $\sigma^{\text{MTUR}}$ and $\sigma$ is observed close to equilibrium (see Fig. 2).
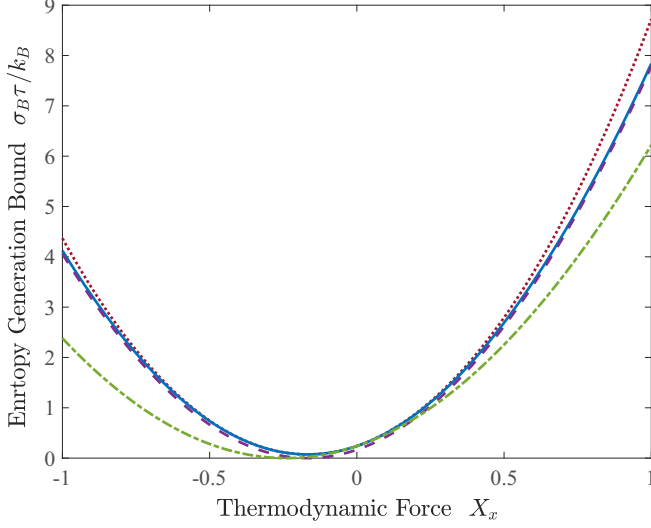
FIG. 1. Entropy generation as a function of applied thermodynamic force $X_x$ in the near equilibrium regime. The dotted (red) line is $\sigma$, the solid (blue) line is $\sigma^{\text{MTUR}}$, and the dashed (purple) and dash-dotted (green) lines are $\sigma_x^{\text{TUR}}$ and $\sigma_y^{\text{TUR}}$, respectively. Parameters are $X_y = 0.2$, $\kappa_{(1,0)} = \kappa_{(0,1)}$, $\kappa_{(1,1)} = 5\kappa_{(1,0)}$, and characteristic time scale $\tau^{-1} = \kappa_{(1,0)}$.

Figure 3 shows an example further from equilibrium. The relative error between $\sigma^{\text{MTUR}}$ and $\sigma$ arises from the finite size of $\kappa_{(1,0)}$ and $\kappa_{(0,1)}$ in this example. Note that despite this discrepancy the MTUR is still a far better bound than the TUR in this regime. From Fig. 3 (inset) we can see that $v_x > 0$ for $-1.4 < X_x < 0$ representing an energy conversion process. It is evident that the constraints on the entropy generation given
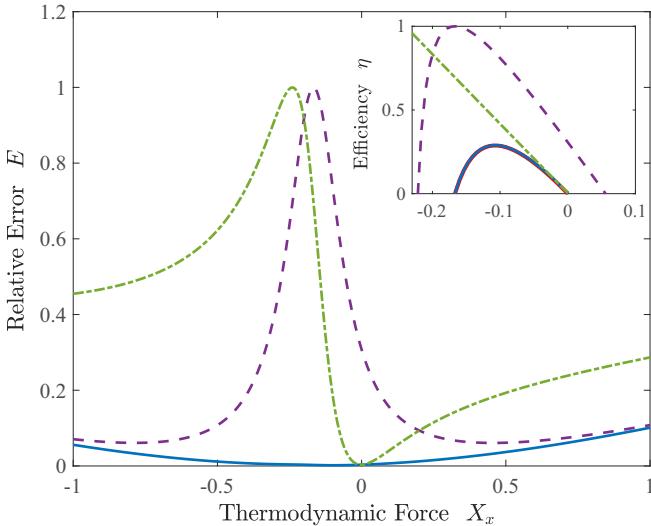


FIG. 2. Relative error in entropy generation and efficiency (inset) as a function of applied thermodynamic force $X_x$ in the near equilibrium regime. The dotted (red) line is $\sigma$ (inset only), the solid (blue) line is $\sigma^{\text{MTUR}}$, and the dashed (purple) and dash-dotted (green) lines are $\sigma_x^{\text{TUR}}$ and $\sigma_y^{\text{TUR}}$, respectively. Parameters are the same as Fig. 1. $v_x > 0$ for $-0.175 < X_x < 0$ represents an energy conversion process.
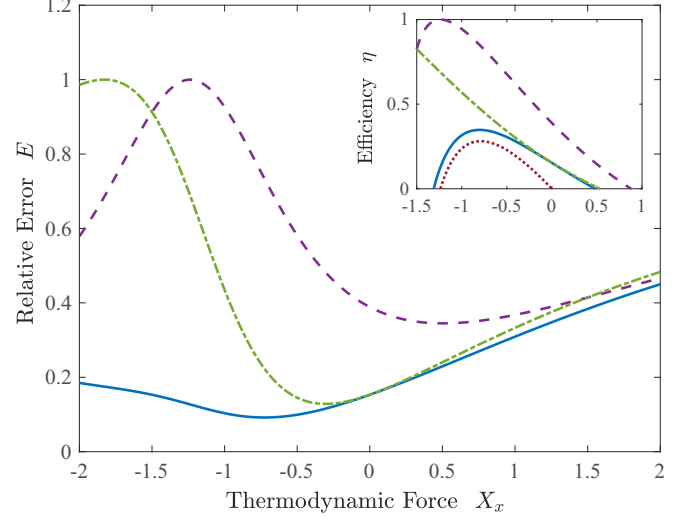


FIG. 3. Relative error in entropy generation and efficiency (inset) as a function of applied thermodynamic force $X_x$. The dotted (red) line is $\sigma$ (inset only), the solid (blue) line is $\sigma^{\text{MTUR}}$, and the dashed (purple) and dash-dotted (green) lines are $\sigma_x^{\text{TUR}}$ and $\sigma_y^{\text{TUR}}$, respectively. Parameters are $X_y = 1.5$, $\kappa_{(1,0)} = \kappa_{(0,1)}$, and $\kappa_{(1,1)} = 5\kappa_{(0,1)}$. $v_x > 0$ for $-1.4 < X_x < 0$ representing an energy conversion process.

by $\sigma_j^{\text{TUR}}$ lead to significant overestimates of the efficiency. For $X_x < -1$ in Fig. 3 (inset) the TUR constraints diverge significantly from the actual entropy generation rate. On the other hand, the efficiency given by $\eta_{\text{B}}(\sigma^{\text{MTUR}})$ provides a much tighter bound.

The TUR and MTUR diverge from the actual entropy production rate for large forces. To understand this divergence let us consider the simple case when only $\kappa_{(1,0)}$ is nonzero. From Eqs. (38) and (39) we have $v_y = 0$, $v_x = 2a_x\kappa_{(1,0)}\sinh(X_x/2)$, $D_{yy} = D_{xy} = 0$, and $D_{xx} = a_x^2\kappa_{(1,0)}\cosh(X_x/2)$. Therefore, $[D^{-1}v]_x a_x = 2\tanh(f_x/2k_BT)$. But this tends to a constant value with large $f_x$, and thus diverges linearly from $f_x$. The ultimate origin of this behavior is the nonlinear behavior arising from the exponential dependence of the hopping rates on barrier height [see Eq. (23)].

Finally, we compare the Stoke's efficiency (17) with the efficiency bound given by

$$\varepsilon_B(\sigma_B) \equiv \frac{\gamma_x v_x^2}{T\sigma_B}, \qquad (41)$$

where $\sigma_B$ is $\sigma^{\text{MTUR}}$ or $\sigma_i^{\text{TUR}}$. Figure 4 shows that, as expected, $\sigma^{\text{MTUR}}$ provides a better bound than $\sigma_x^{\text{TUR}}$.

## VI. BEYOND THE DEEP-WELL REGIME

For more general potentials we need a method of determining $v$ and $D$ numerically. Using the Bloch state description we can show that $u_{k,\alpha}(r)$ satisfies

$$[\mathcal{L} - k_B T k^{\mathsf{T}} M k + i\chi^{\mathsf{T}} k] u_{k,\alpha}(r) = -\lambda_{k,\alpha} u_{k,\alpha}(r), \qquad (42)$$

where $\chi = M\{2k_B T \nabla + [\nabla V(r)]\}$. This operator equation can be evaluated numerically to find $\lambda_{k,\alpha}$. As the potential and $u_{k,\alpha}(r)$ are periodic functions, it is convenient to carry this out
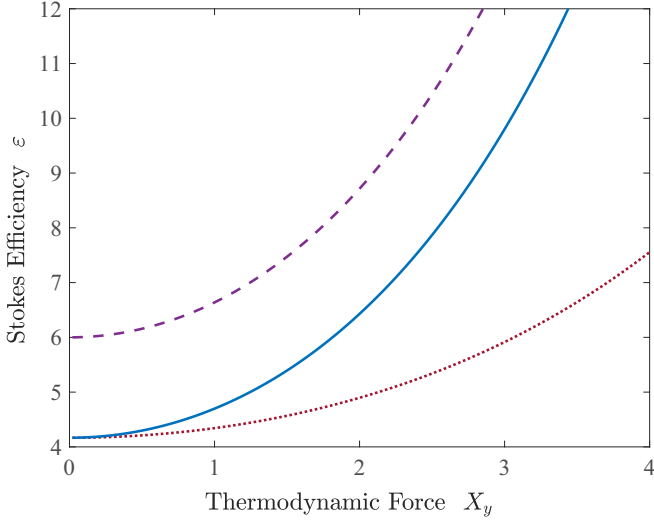
FIG. 4. Stokes efficiency and bounds as a function of applied thermodynamic force $X_y$. The dotted (red) line is $\sigma$, the solid (blue) line is $\sigma^{\text{MTUR}}$, and the dashed (purple) line is $\sigma_x^{\text{TUR}}$. Parameters are $X_x = 0$, $\kappa_{(1,0)} = \kappa_{(0,1)}$, and $\kappa_{(1,1)} = 5\kappa_{(0,1)}$.

in $k$ space. Solving the eigensystem is then straightforward using standard techniques. The drift and diffusion can then be calculated in $k$ space using finite difference estimates of Eqs. (25) and (26).

As a simple example potential we consider

$$V_0(\mathbf{r}) = -V_x \cos(2\pi x/a_x) - V_y \cos(2\pi y/a_y)$$
$$- V_z \cos[2\pi(x/a_x - y/a_y)]. \quad (43)$$

As noted previously, the deep-well limit described by a master equation (Sec. V) is only valid for small forces and cannot be used to explore the regime where the force is larger than the confining barriers. In Fig. 5 we show the performance of the error bounds for the potential (43) with large forces. Parameters are chosen to approximately coincide with the limiting case shown in Fig. 2 close to $X_x = 0$. Figure 5 shows that the MTUR provides a good bound on the entropy close to equilibrium and for very large forces, but is inaccurate in the intermediate regime and diverges from the actual entropy generation at the critical point: $X_x/2\pi \approx -\Delta V/k_B T$, where the potential barriers in $V(\mathbf{r})$ vanish. This result is known from one dimensional treatments [20].

To understand these results we note that from Eq. (10) we can see that entropy generation is minimized when it is equal to the MTUR. In this case $\mathbf{v}^\mathsf{T}\mathbf{f} = k_B T \mathbf{v}^\mathsf{T} D^{-1}\mathbf{v}$, or

$$\mathbf{v} = D\mathbf{f}/k_B T. \quad (44)$$

The minimization of the entropy generation in the linear regime ($\mathbf{v} \propto \mathbf{f}$) has been discussed previously [1,2,20] in the context of Eq. (8). Equation (44) holds close to equilibrium $\mathbf{f} \to 0$ when $D = D(\mathbf{f} = 0)$ [1,2] and far from equilibrium when $|\mathbf{f}^\mathsf{T}\mathbf{a}|$ is much larger than the barriers in $V(\mathbf{r})$ [20]. For large enough forces the potential is well described by a linear potential with a periodic perturbation and Eq. (44) holds. As shown in Fig. 5, for intermediate forces, the MTUR (and the TUR) diverge from the actual entropy production rate. This results from the difference between $\mathbf{f}$ and $D^{-1}\mathbf{v}$ [cf.
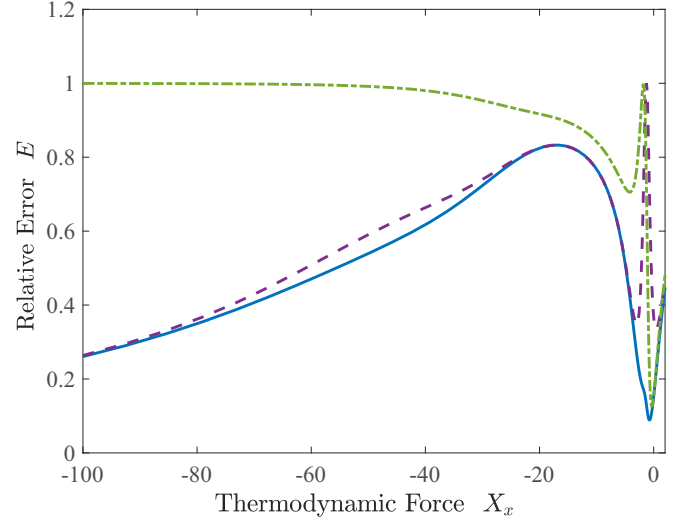
Eq. (44)]. An argument similar to that given in Sec. V also holds for more complicated cases. For example, comparing $[D^{-1}\mathbf{v}]_x a_x$ with $X_x$ in Fig. 6 (for the same parameters as Fig. 5) we see that $[D^{-1}\mathbf{v}]_x a_x$ becomes approximately constant and thus diverges from $X_x$ as $|X_x| \gg 1$. For even greater forces the approximations in Sec. V break down and this divergence reaches its peak. For even higher forces the relative error decreases until eventually the minimum uncertainty relation (44) holds again. The large growth in the diffusion close to the critical point in the one dimensional case is well known [26–28].
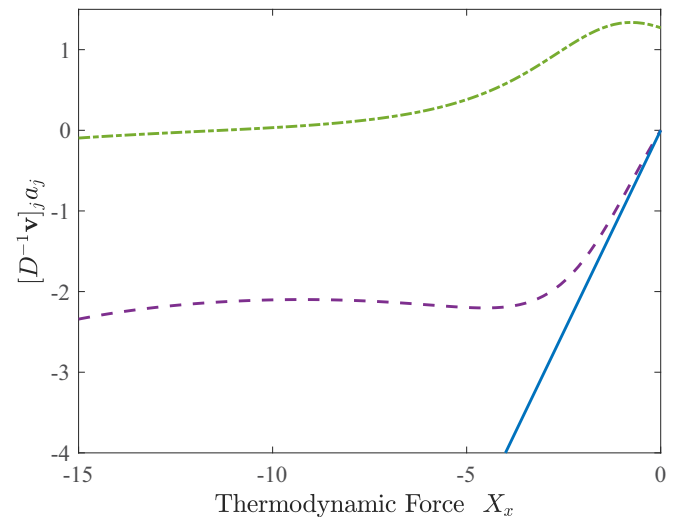


FIG. 5. Relative error in entropy generation as a function of applied thermodynamic force $X_x$. The solid line (blue) is $\sigma^{\text{MTUR}}$ and the dashed (purple) and dash-dotted (green) lines are $\sigma_x^{\text{TUR}}$ and $\sigma_y^{\text{TUR}}$, respectively. Parameters are chosen to approximately coincide with the limiting case shown in Fig. 2: $\gamma_y = \gamma_x$, $a_x = a_y$, $V_x = 2k_B T$, $V_y = 2k_B T$, $V_z = 3.8k_B T$, and $X_y = 1.5$. Similar to Fig. 2, $v_x > 0$ for $-1.25 < X_x < 0$ represents an energy conversion process.



FIG. 6. Plot of $[D^{-1}\mathbf{v}]_x a_x$ dashed (purple) line and $[D^{-1}\mathbf{v}]_y a_y$ dash-dotted (green) line as a function of $X_x$. The solid (blue) line shows $X_x$. Parameters are the same as in Fig. 5.
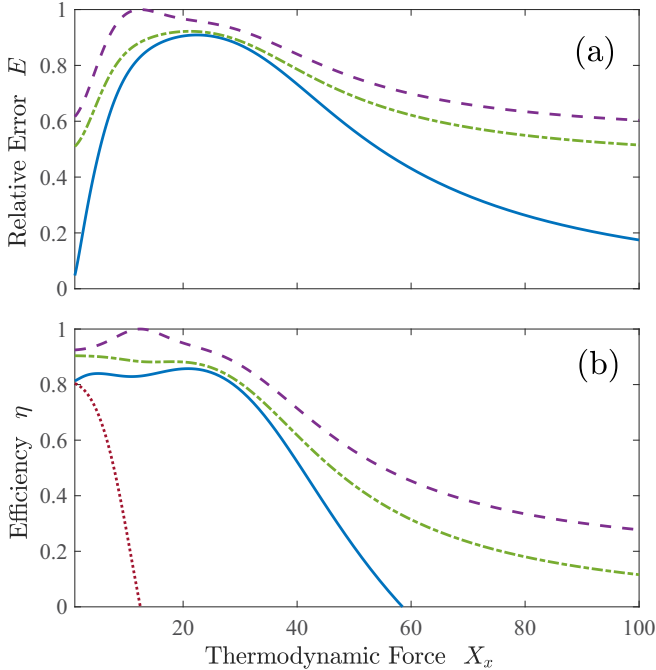
FIG. 7. Relative error in entropy generation (a) and thermodynamic efficiency (b) as a function of applied thermodynamic force $X_x$. The solid line (blue) is for $\sigma^{\text{MTUR}}$, the dotted line (red) is for $\sigma$ [only in (b)], and the dashed (purple) and dash-dotted (green) lines are for $\sigma_x^{\text{TUR}}$ and $\sigma_y^{\text{TUR}}$, respectively. Parameters are $\gamma_y = \gamma_x$, $V_x = 1k_B T$, $V_y = 1k_B T$, $V_z = 5k_B T$, and $X_y = -1.1X_x$. For these parameters $v_x > 0$ for $X_x < 13$ representing an energy conversion process.

In general, energy conversion does not occur in the large force regime as potential barriers are required to induce a drift against an applied force. A particularly interesting case occurs for a tightly bound diagonal potential channel [$V_z \gg V_x, V_y$ in Eq. (43)], where $X_x$ is increased holding $X_x \approx -X_y$. This creates a minimum uncertainty state with high energy conversion efficiency ($v_x \approx v_y$) for small forces but, for sufficiently large forces, the barriers inducing the energy conversion become smaller than the external force. Figure 7(a) shows the relative error between the MTUR and TUR and the entropy in this case. Similar to Fig. 5 the MTUR diverges close to the critical point where the bound state vanishes. In this case the efficiency is very high for small forces [see Fig. 7(b)]. The $\sigma^{\text{MTUR}}$ and $\sigma_j^{\text{TUR}}$ bounds on the efficiency are particularly inaccurate in this case.

## VII. TRADE-OFF BETWEEN PRECISION AND DISSIPATION

The above results also have implications for the trade-off between precision and dissipation. We have shown that the MTUR provides a multidimensional generalization of the TUR so in this section we confine our discussion to the MTUR. In small and very large force regimes where the minimum uncertainty condition Eq. (44) approximately holds, then

$$\sigma \gtrsim \sigma^{\text{MTUR}} = k_B \boldsymbol{v}^{\mathsf{T}} D^{-1} \boldsymbol{v}. \tag{45}$$

In these regimes, it is reasonable to interpret the MTUR as meaning that greater relative precision requires greater dissipation. However, in the intermediate force regime, the MTUR diverges from the actual entropy production rate (see Figs. 5 and 7). Due to this divergence between the actual entropy production rate and $\sigma^{\text{MTUR}}$ in this regime, there are large sources of entropy generation beyond that required to ensure relative precision and the trade-off becomes less relevant.

One of the arguments for the usefulness of the TUR is that measurements of the diffusion and drift in one dimension would provide a bound on the entropy generation rate [10]. The diffusion and drift can be estimated from experimentally measured single-molecule trajectories (e.g., Ref. [26]). However, in many cases the TUR places only a loose bound on the entropy generation rate. The MTUR places a much tighter bound; however, its calculation would require measurement of the drift and diffusion in each relevant degree of freedom and the correlation between the two. It is not clear how this could be achieved if one of the degrees of freedom is a chemical coordinate. In addition, if the force in each degree of freedom is known, then determining the entropy generation directly via Eq. (7) would be much more straightforward. If the force is not known then the MTUR could be an option for estimating a bound.

## VIII. CONCLUSION

In this paper we have considered a description of molecular-scale energy conversion in terms of continuous Brownian motion on a time-independent periodic potential that explicitly includes the degrees of freedom exchanging energy. We have compared the TUR [1] and the recently derived MTUR [11] to the entropy generation of this system.

First, we have shown that the MTUR has a clear physical interpretation in terms of course-grained dynamics of the system (see Sec. III), is consistent with the original TUR (see Sec. IV), but always represents a tighter bound on the entropy generation.

Our second finding is that the TUR, although providing a universal lower bound on the entropy generation, is often a very weak bound in regimes relevant to energy conversion. The original TUR has been used to derive an upper bound on efficiency [9,10]. However, as a consequence of the TUR providing a weak bound on entropy generation, it significantly overestimates the efficiency in a number of regimes including the deep well regime where the TUR was originally derived. As a consequence of the MTUR providing a tighter lower bound on entropy generation, it also provides a tighter upper bound on the thermodynamic efficiency. These attributes make the MTUR the natural multidimensional generalization of the TUR especially for applications involving energy conversion. This stems from the fact that it takes into account the correlations between degrees of freedom that arise in energy conversion processes.

As a third result we have shown that both the TUR and the MTUR diverge from the entropy generation rate in the intermediate force regime where the externally applied force is close to the force of local confining barriers. The same behavior was found for the TUR in one dimension [20]; however, it has important ramifications for the MTUR as an

efficiency bound in higher dimensions (see Fig. 7). Thus the MTUR is most useful as a bound on the entropy close to and very far from thermal equilibrium. In both these cases the linear relation between the drift and force holds. However, both the TUR and the MTUR diverge from the entropy generation in the intermediate force regime between these two cases. In this regime there is a strongly nonlinear relation between the drift, the diffusion, and the force. Hence the TUR and MTUR relations, while providing universal bounds, in some regimes are too weak to be useful.

Finally, we have considered the consequences of these results for the trade-off between precision and dissipation. Our results show that in the small and very large force regimes where the minimum uncertainty state is approximately valid, it is reasonable to interpret the MTUR as meaning that greater relative precision requires greater dissipation. However, in the intermediate force regime, the actual entropy rate diverges from the MTUR, showing that sources of entropy generation beyond that required to ensure precision dominate and this interpretation loses predictive power.

## APPENDIX A

In the special case described in Sec. II the lowest band eigenvalues take the form

$$
\begin{aligned}
\lambda_{\boldsymbol{k},0} = {} & 4\kappa^0_{(1,0)} G_{(1,0)}(X_x) \sin\left(\tfrac{1}{2}k_x a_x\right) \sin\left(\tfrac{1}{2}k_x a_x + i\tfrac{1}{2}X_x\right) \\
& + 4\kappa^0_{(0,1)} G_{(0,1)}(X_y) \sin\left(\tfrac{1}{2}k_y a_y\right) \sin\left(\tfrac{1}{2}k_y a_y + i\tfrac{1}{2}X_y\right) \\
& + 4\kappa^0_{(1,1)} G_{(1,1)}(X_+) \sin\left(\tfrac{1}{2}k_x a_x + \tfrac{1}{2}k_y a_y\right) \\
& \times \sin\left(\tfrac{1}{2}k_x a_x + \tfrac{1}{2}k_y a_y + i\tfrac{1}{2}X_+\right) \\
& + 4\kappa^0_{(1,-1)} G_{(1,-1)}(X_-) \sin\left(\tfrac{1}{2}k_x a_x - \tfrac{1}{2}k_y a_y\right) \\
& \times \sin\left(\tfrac{1}{2}k_x a_x - \tfrac{1}{2}k_y a_y + i\tfrac{1}{2}X_-\right),
\end{aligned}
\tag{A1}
$$

where $G_{\boldsymbol{n}}(x) = e^{(\alpha^0_{\boldsymbol{n}} - 1/2)x}$, $X = Af/k_B T$, and $X_\pm = X_x \pm X_y$.

The drift and diffusion are then calculated from Eqs. (25) and (26) to be

$$
\begin{aligned}
v_x/a_x = {} & 2\kappa^0_{(1,0)} G_{(1,0)}(X_x/2) \sinh(X_x/2) \\
& + 2\kappa^0_{(1,1)} G_{(1,1)}(X_+/2) \sinh(X_+/2) \\
& + 2\kappa^0_{(1,-1)} G_{(1,-1)}(X_-/2) \sinh(X_-/2),
\end{aligned}
\tag{A2a}
$$

$$
\begin{aligned}
v_y/a_y = {} & 2\kappa^0_{(0,1)} G_{(0,1)}(X_y/2) \sinh(X_y/2) \\
& + 2\kappa^0_{(1,1)} G_{(1,1)}(X_+/2) \sinh(X_+/2) \\
& - 2\kappa^0_{(1,-1)} G_{(1,-1)}(X_-/2) \sinh(X_-/2)
\end{aligned}
\tag{A2b}
$$

and

$$
\begin{aligned}
\frac{D_{xx}}{a_x^2} = {} & \kappa^0_{(1,0)} G_{(1,0)}(X_x/2) \cosh(X_x/2) \\
& + \kappa^0_{(1,1)} G_{(1,1)}(X_+/2) \cosh(X_+/2) \\
& + \kappa^0_{(1,-1)} G_{(1,-1)}(X_-/2) \cosh(X_-/2),
\end{aligned}
\tag{A3a}
$$

$$
\begin{aligned}
\frac{D_{yy}}{a_y^2} = {} & \kappa^0_{(0,1)} G_{(0,1)}(X_y/2) \cosh(X_y/2) \\
& + \kappa^0_{(1,1)} G_{(1,1)}(X_+/2) \cosh(X_+/2)
\end{aligned}
$$

$$
\begin{aligned}
& + \kappa^0_{(1,-1)} G_{(1,-1)}(X_-/2) \cosh(X_-/2),
\end{aligned}
\tag{A3b}
$$

$$
\begin{aligned}
\frac{D_{xy}}{a_x a_y} = \frac{D_{yx}}{a_x a_y} = {} & \kappa^0_{(1,1)} G_{(1,1)}(X_+/2) \cosh(X_+/2) \\
& - \kappa^0_{(1,-1)} G_{(1,-1)}(X_-/2) \cosh(X_-/2).
\end{aligned}
\tag{A3c}
$$

The drift and diffusion of this system has been explored previously [21], but not in the context of the TURs. A simplified version of these equations with $\kappa^0_{(1,-1)} = 0$ and $\alpha^0_{\boldsymbol{n}} = 1/2$ is presented in the main text. The conclusions do not depend on these simplifications.

## APPENDIX B

In this Appendix we aim to show that

$$
\boldsymbol{v} D^{-1} \boldsymbol{v} \geqslant \frac{v_1^2}{D_{11}}
\tag{B1}
$$

holds in in $N$ dimensions, where we have chosen a convenient ordering of the indices. A few results from block matrices
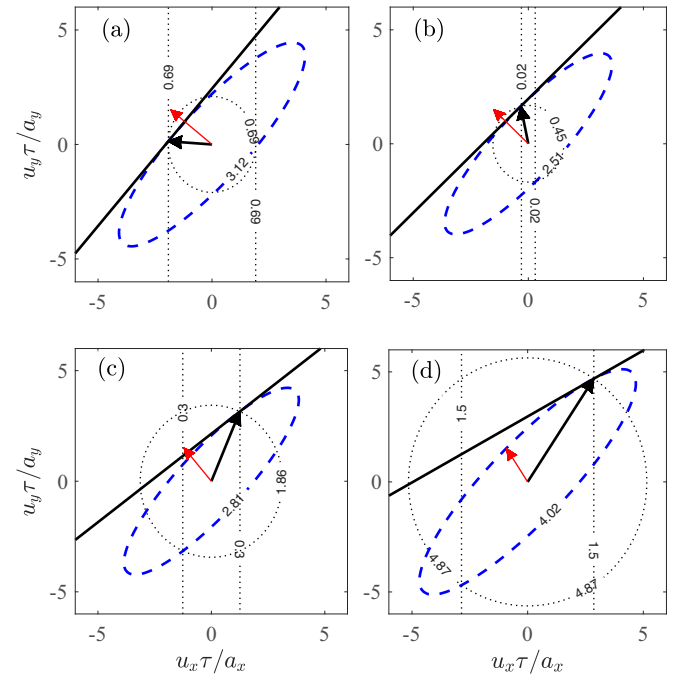


FIG. 8. Contour plot of the functions (C1) for different values of applied forces. The solid (black) line is $g(\boldsymbol{u})$, the dotted vertical lines are $g_x^{\mathrm{TUR}}(\boldsymbol{u})$, the dotted ellipse is $g^{\mathrm{diag}}(\boldsymbol{u})$, and the dashed rotated ellipse corresponds to $g^{\mathrm{MTUR}}(\boldsymbol{u})$. The (red) thin arrow is the force $A\boldsymbol{f}/k_B T$ and the (black) thick arrow is the drift $\tau A^{-1}\boldsymbol{v}$. Contour values are in units of $\tau^{-1} = \kappa_{(0,1)}$, a characteristic rate of the system. Only one contour is shown for each function and corresponds to the values when $\boldsymbol{u} = \boldsymbol{v}$ and thus all functions intersect with the drift vector. The values of force and resulting $g(\boldsymbol{v})$ are (a) $A\boldsymbol{f}/k_B T = (-1.8, 1.5)$ and $g(\boldsymbol{v}) = 3.66\tau^{-1}$, (b) $A\boldsymbol{f}/k_B T = (-1.5, 1.5)$ and $g(\boldsymbol{v}) = 2.96\tau^{-1}$, (c) $A\boldsymbol{f}/k_B T = (-1.2, 1.5)$ and $g(\boldsymbol{v}) = 3.22\tau^{-1}$, and (d) $A\boldsymbol{f}/k_B T = (-0.9, 1.5)$ and $g(\boldsymbol{v}) = 4.46\tau^{-1}$. Other parameters are $\kappa_{(1,1)} = 5\kappa_{(0,1)}$, $\kappa_{(1,0)} = 0.2\kappa_{(0,1)}$, and $\alpha_j = 0$. See Sec. V for more details of the parameters.

assist with this proof [29]. In block matrix form we can write

$$D = \begin{bmatrix} D_{11} & \boldsymbol{B}^{\mathsf{T}} \\ \boldsymbol{B} & \bar{D}_{11} \end{bmatrix}, \tag{B2}$$

where $D_{11}$ is the $j' = 1$, $j = 1$ element of $D$, $\boldsymbol{B}$ is a $1 \times N$ vector with components $B_j = D_{j1}$, and $\bar{D}_{11}$ is the $(N-1) \times (N-1)$ lower right-hand block of $D$. We can write the block matrix form of $D$ as

$$\begin{bmatrix} D_{11} & \boldsymbol{B}^{\mathsf{T}} \\ \boldsymbol{B} & \bar{D}_{11} \end{bmatrix} = \begin{bmatrix} 1 & 0 \\ D_{11}^{-1}\boldsymbol{B} & \mathbb{1}_{N-1} \end{bmatrix}$$
$$\times \begin{bmatrix} D_{11} & 0 \\ 0 & K \end{bmatrix} \begin{bmatrix} 1 & D_{11}^{-1}\boldsymbol{B}^{\mathsf{T}} \\ 0 & \mathbb{1}_{N-1} \end{bmatrix}, \tag{B3}$$

where $K = \bar{D}_{11} - D_{11}^{-1}\boldsymbol{B}\boldsymbol{B}^{\mathsf{T}}$. The inverse of $D$ in block form is

$$D^{-1} = \begin{bmatrix} D_{11} & \boldsymbol{B}^{\mathsf{T}} \\ \boldsymbol{B} & \bar{D}_{11} \end{bmatrix}^{-1}. \tag{B4}$$

Taking the inverse of each matrix on the right-hand side of Eq. (B3) we can show that

$$\begin{bmatrix} D_{11} & \boldsymbol{B}^{\mathsf{T}} \\ \boldsymbol{B} & \bar{D}_{11} \end{bmatrix}^{-1} = \begin{bmatrix} D_{11}^{-1} + D_{11}^{-2}\boldsymbol{B}^{\mathsf{T}}K^{-1}\boldsymbol{B} & -D_{11}^{-1}\boldsymbol{B}^{\mathsf{T}}K^{-1} \\ -D_{11}^{-1}K^{-1}\boldsymbol{B} & K^{-1} \end{bmatrix}. \tag{B5}$$

To show that Eq. (B1) holds in $N$ dimensions it suffices to show that the $N \times N$ matrix $A$,

$$A = \begin{bmatrix} D_{11} & \boldsymbol{B}^{\mathsf{T}} \\ \boldsymbol{B} & \bar{D}_{11} \end{bmatrix}^{-1} - \begin{bmatrix} D_{11}^{-1} & 0 \\ 0 & 0 \end{bmatrix}, \tag{B6}$$

is positive semidefinite.

From Eq. (B5), $A$ can be written as

$$A = \begin{bmatrix} D_{11}^{-2}\boldsymbol{B}^{\mathsf{T}}K^{-1}\boldsymbol{B} & -D_{11}^{-1}\boldsymbol{B}^{\mathsf{T}}K^{-1} \\ -D_{11}^{-1}K^{-1}\boldsymbol{B} & K^{-1} \end{bmatrix} \tag{B7}$$

$$= \begin{bmatrix} -D_{11}^{-1}\boldsymbol{B}^{\mathsf{T}} \\ \mathbb{1}_{N-1} \end{bmatrix} K^{-1} \begin{bmatrix} -D_{11}^{-1}\boldsymbol{B} & \mathbb{1}_{N-1} \end{bmatrix}. \tag{B8}$$

As $D$ is positive definite each block of the block diagonal matrix [middle matrix on the right-hand side of Eq. (B3)] must be positive definite; thus $K$ is positive definite. Since $K$ is positive definite so is $K^{-1}$ and we can write $K^{-1} = RR^{T}$. This means that we can also write $A = R'R'^{\mathsf{T}}$, where

$$R' = \begin{bmatrix} -D_{11}^{-1}\boldsymbol{B}^{\mathsf{T}} \\ \mathbb{1}_{N-1} \end{bmatrix} R. \tag{B9}$$

This shows that $A$ must be at least positive semidefinite, which concludes the proof.

## APPENDIX C

It is useful to understand the functional structure of the various quantities that we have introduced in this paper. To help with this we define the following functions of $\boldsymbol{u}$:

$$g(\boldsymbol{u}) = \frac{\boldsymbol{u}^{\mathsf{T}}\boldsymbol{f}}{k_B T}, \tag{C1a}$$

$$g_x^{\mathrm{TUR}}(\boldsymbol{u}) = \frac{u_x^2}{D_{xx}}, \tag{C1b}$$

$$g^{\mathrm{diag}}(\boldsymbol{u}) = \frac{u_x^2}{D_{xx}} + \frac{u_y^2}{D_{yy}}, \tag{C1c}$$

$$g^{\mathrm{MTUR}}(\boldsymbol{u}) = \boldsymbol{u}^{\mathsf{T}}D^{-1}\boldsymbol{u}, \tag{C1d}$$

reflecting the quantities $\sigma/k_B$, $\sigma_x^{\mathrm{TUR}}/k_B$, $\sum_j \frac{v_j^2}{k_B D_{jj}}$, and $\sigma^{\mathrm{MTUR}}/k_B$, respectively. Plotted as a function of $u_x$ and $u_y$ in two dimensions, $g(\boldsymbol{u})$ represents an inclined plan with normal vector $(f_x a_x/k_B T, f_y a_y/k_B T, -1)$, $g_x^{\mathrm{TUR}}(\boldsymbol{u})$ a parabolic cylinder with no variation in $u_y$, $g^{\mathrm{diag}}(\boldsymbol{u})$ is an elliptic paraboloid, and $g^{\mathrm{MTUR}}(\boldsymbol{u})$ a rotated elliptic paraboloid. Contour plots of these quantities are shown in Fig. 8 for different values of the thermodynamic force $\boldsymbol{f}$. Section V describes how $D$ and $\boldsymbol{v}$ in these figures are calculated.

Figure 8 shows examples with significant off-diagonal components of $D$. In these examples, $f_y > 0$ is constant and $f_x < 0$ increases from (a) to (d). In each case, the curvature of $g_x^{\mathrm{TUR}}(\boldsymbol{u})$ is such that it underestimates the entropy generation. Figure 8(a) shows an example of high entropy production; $\boldsymbol{f}$ is almost parallel to $\boldsymbol{v}$, with no energy conversion, $v_x < 0$. Both $g_x^{\mathrm{TUR}}(\boldsymbol{u} = \boldsymbol{v})$ and $g^{\mathrm{diag}}(\boldsymbol{u} = \boldsymbol{v})$ underestimate the entropy generation rate $g(\boldsymbol{u} = \boldsymbol{v})$. Figure 8(b) shows a case where $f_y$ is reduced to the point where $v_x \approx 0$. In this case $g_x^{\mathrm{TUR}}(\boldsymbol{u} = \boldsymbol{v}) \approx 0$ and represents a very inaccurate bound on the entropy generation. Figures 8(c) and 8(d) show cases with energy conversion $v_x > 0$. In Fig. 8(d), where large energy conversion is occurring, $g^{\mathrm{diag}}(\boldsymbol{u} = \boldsymbol{v})$ overestimates the entropy generation rate.

[1] A. C. Barato and U. Seifert, Phys. Rev. Lett. **114**, 158101 (2015).

[2] T. R. Gingrich, J. M. Horowitz, N. Perunov, and J. L. England, Phys. Rev. Lett. **116**, 120601 (2016).

[3] A. C. Barato and U. Seifert, J. Phys. Chem. B **119**, 6555 (2015).

[4] K. Brandner, T. Hanazato, and K. Saito, Phys. Rev. Lett. **120**, 090601 (2018).

[5] A. Rosas, C. Van den Broeck, and K. Lindenberg, Phys. Rev. E **96**, 052135 (2017).

[6] L. P. Fischer, P. Pietzonka, and U. Seifert, Phys. Rev. E **97**, 022143 (2018).

[7] A. C. Barato and U. Seifert, Phys. Rev. X **6**, 041053 (2016).

[8] P. Pietzonka and U. Seifert, Phys. Rev. Lett. **120**, 190602 (2018).

[9] W. Hwang and C. Hyeon, J. Phys. Chem. Lett. **9**, 513 (2018).

[10] P. Pietzonka, A. C. Barato, and U. Seifert, J. Stat. Mech. **12** (2016)124004.

[11] A. Dechant, J. Phys. A: Math. Theor. **52**, 035001 (2019).

[12] M. O. Magnesco, Phys. Rev. Lett. **72**, 2656 (1994).

[13] D. Keller and C. Bustamante, Biophys. J. **78**, 541 (2000).

[14] K. J. Challis and M. W. Jack, Phys. Rev. E **88**, 042114 (2013).

[15] R. D. Astumian, Phys. Chem. Chem. Phys. **9**, 5067 (2007).

[16] C. W. Gardiner, *Stochastic Methods: A Handbook for the Natural and Social Sciences*, 4th ed. (Springer-Verlag, New York, 2009).

[17] C. Van den Broeck and M. Esposito, Phys. Rev. E **82**, 011144 (2010).

[18] T. Tomé and M. J. de Oliveira, Phys. Rev. E **82**, 021120 (2010).

[19] M. W. Jack and C. Tumlin, Phys. Rev. E **93**, 052109 (2016).

[20] C. Hyeon and W. Hwang, Phys. Rev. E **96**, 012156 (2017).

[21] K. J. Challis and M. W. Jack, Phys. Rev. E **88**, 062136 (2013).

[22] P. Reimann, Phys. Rep. **361**, 57 (2002).

[23] H. Wang and G. F. Oster, Europhys. Lett. **57**, 134 (2002).

[24] C. Kittel, *Introduction to Solid State Physics* (Wiley, New York, 2004).

[25] K. J. Challis, Phys. Rev. E **97**, 062158 (2018).

[26] R. Hayashi, K. Sasaki, S. Nakamura, S. Kudo, Y. Inoue, H. Noji, and K. Hayashi, Phys. Rev. Lett. **114**, 248101 (2015).

[27] P. Reimann, C. Van den Broeck, H. Linke, P. Hänggi, J. M. Rubi, and A. Pérez-Madrid, Phys. Rev. Lett. **87**, 010602 (2001).

[28] P. Reimann, C. Van den Broeck, H. Linke, P. Hänggi, J. M. Rubi, and A. Pérez-Madrid, Phys. Rev. E **65**, 031104 (2002).

[29] P. Lancaster and M. Tismenetsky, *The Theory of Matrices*, 2nd ed. (Academic Press, San Diego, 1985).